The Aeronautical Journal (2023), **127**, pp. 116–138
doi:10.1017/aer.2022.35

REGULAR PAPER

Dynamic responses due to the Dryden gust of an autonomous quadrotor UAV carrying a payload

R. S. Geronel[1,*], R. M. Botez[2] and D. D. Bueno[1]

[1]São Paulo State University (UNESP), School of Engineering of Ilha Solteira, Ilha Solteira, Brazil and [2]Research Laboratory in Active Control, Avionics and AeroServoElasticity (LARCASE), Ecole de Technologie Superieure, Montreal, Canada
*Corresponding author. Email: renan.sanches@unesp.br

Received: 18 August 2021; **Revised:** 12 February 2022; **Accepted:** 14 March 2022

Keywords: Unmanned Aerial Vehicle; Payload; Sliding Mode Control; Proportional Derivative; Vibration Control; Dryden gust

Abstract

Unmanned Aerial Vehicles (UAVs) have been used extensively in many applications, such as surveillance, medical transportation and delivery tasks. These applications usually involve an attachment system to connect a payload. However, when connected to such a coupled system, the UAV exhibits lower flight performance mainly due to gust loads. Mathematical modeling is used in this paper to illustrate the comparison between an UAV with a coupled system and a conventional UAV. Proportional Derivative (PD) and Sliding Mode Control (SMC) approaches are used to evaluate the vibrations of the payload, and the UAV trajectory subjected to Dryden gust. This work therefore uses these methods to investigate the dynamic response of a quadrotor-type UAV equipped with a payload and a flexible attachment system.

Nomenclature

X_M, Y_M, Z_M	body-fixed reference frame
F_{jj}	generated forces on each propeller
T_{jj}	generated torque on each propeller
m	mass of the quadrotor
m_c	mass of the payload
k_c	stiffness between the quadrotor and its payload
x,y,z	positions of the quadrotor
$x_{des}, y_{des}, z_{des}$	desired positions of the quadrotor
z_c	vertical position of the payload
U_{1c}, U_2, U_3, U_4	inputs control
g	gravitational vector
s_{ii}	sliding surfaces, where $ii = x, y, z, \phi\, \theta, \psi$
e_{ii}	error between the desired and current state variable
I_{ii}	moment of inertia of the quadrotor
I^c_{ii}	moment of inertia of the payload
L_{ii}	Dryden turbulence scale length, where $kk = x, y, z$
V	wind velocity
C_{dz}	drag coefficient
A_z	area projected by the UAV

Greek Symbols

ω_{kk}	angular rotation
ϕ, θ, ψ	orientation angles of the quadrotor
$\phi_{des}, \theta_{des}, \psi_{des}$	desired orientation angles of the quadrotor

λ_{ii}	tuning coefficient associated with the closed loop
ϵ_{ii}	controller positive parameters
η_{ii}	positive real coefficients of the controller
γ	transition bandwidth coefficient
Φ_{kk}	power spectral density
σ_{kk}	Dryden turbulenece intensity
ω_{ws}	mean wind speed
ρ	air density

Acronym list

UAVs	Unmanned Aerial Vehicles
SMC	Sliding Mode Control
PD	Proportional Derivative
GMT	Ground Moving Target
CA	Control Allocation
MAVs	Multi-Aerial Vehicles
FDD	Fault Detection and Diagnosis
LQR	Linear Quadratic Regulator
ASMC	Adaptive Sliding Mode Control
IAE	Integral of the Absolute magnitude of the Error
ITAE	Integral of Time multiplied by the Absolute Error
PSD	Power Spectral Density
FFT	Fast Fourier Transform

1.0 Introduction

Unmanned Aerial Vehicles (UAVs) have experienced significant growth in the past several years due to their increasing number of applications and to the use of their related continuous improved technology (sensors, cameras, processors). The ability to carry a variety of payloads enables a UAV to perform tasks in multiple scenarios, such as military operations, aerial photography, surveillance [1], monitoring traffic flow [2], environmental monitoring [3–5], rapid transport of medicine [6] and delivery tasks in general [7–10]. One of the main applications of UAVs include the commercial delivery of packages, including the transportation of medication, supplies and fragile substances to remote areas [11]. Compared to its conventional design (with no payload), the UAV transportation system presents additional challenges, mainly due to the difficulties encountered by suspended payloads, such as much stronger nonlinearities, as well as more complex adverse dynamic coupling [12].

There are several UAV studies focusing on designing their controllers to fly along a desired trajectory, and to reduce the residual vibration. The constraint forces and moments caused by the connections between the quadrotor and its payload were studied to analyse their influence. In Ref. [13], the payload was attached to a UAV by using a single wire, and a stabilisation method based on PD control was utilised to attenuate the payload oscillations, as well as to obtain the desired flight trajectory. In the presence of the payload stabilisation method, the oscillations are significantly decreased compared to the absence case. In addition, the quadrotor position is well converged into the desired points.

A target tracking algorithm was developed in Ref. [14], based on Sliding Mode Control, for a UAV to track a Ground Moving Target (GMT). The purpose of the algorithm was to maintain a circular motion with respect to the GMT during its UAV trajectory. It is supposed to sense its own states and estimates the GMT. The tracking algorithm is based on SMC, which allows regulating the relative displacements between the UAV and the GMT, in terms of position, velocity and acceleration of the target. However, a camera can also be attached to the UAV as an on-board observation sensor to estimate all its system states and to improve the target tracking process. This camera must have great stability regardless of the environmental disturbances and manoeuvers of the UAV, in order to guarantee an accurate state response of the algorithm.

https://doi.org/10.1017/aer.2022.35 Published online by Cambridge University Press

The Sliding Mode Control (SMC) has been investigated due to its robustness for trajectories tracking under external disturbances [15]. A second-order SMC was validated under different scenarios, where external disturbances were used as adverse conditions. Numerical simulations and experimental tests were performed and revealed that SMC improved the controller performance (when compared to the PID performance), while minimising the overshoot and steady-state errors, even in the presence of significant wind speeds [16]. The SMC strategy based on the adaptation of the switching matrix was used to design the attitude control law for a UAV(17). The switching matrix is a diagonal matrix with three elements (corresponding to each degree of freedom of the attitude control), which can be adjusted individually according to the proposed flight trajectory. This strategy was proposed to evaluate the controller performance under external disturbances and to model its uncertainties, while conducting to a fast and precise convergence to the altitude variables.

The combination of the Fast Non-Singular Terminal Sliding Mode Control (FNTSMC) and Control Allocation (CA) strategies was investigated to verify the flight performance of Multi-Rotor Aerial Vehicles (MAVs) subjected to external disturbance. It can be used for any aerial vehicle, while the control allocation was responsible for generating the 3-D attitude, and computing individual thrust commands, the FNTSMC technique was used to design the geometric position and attitude control laws. This strategy minimised the thrust commands, as well as guaranteed singularity-free convergence, finite-time stability and robustness against disturbances. A 3-DOF hover experiment was used to validate the proposed control, and it has shown positive control responses despite of bounded force (defined by known parameters) and torque disturbances [18].

A robust actuator Fault Detection and Diagnosis (FDD) scheme for a UAV was designed in Ref. [19]. This method has been tested for several conditions, including external disturbances acting on the UAV as well as partial losses in specific motors. This perturbation that the UAV is subjected to (caused by fault and disturbances), might increase exponentially the UAV vibration and its transported mass, which would affect the onboard accuracy, and decrease its flight performance.

Embedded cameras in UAVs were widely used to estimate their positions and velocities; however, they can also be used to estimate their attitude. A downward-facing strapdown camera was used to take landmarks pictures and determine pairs of vector measurements (from the camera to the landmark). The proposed method investigated the measurements determination, and the technique was divided into three modules: the first module used to detect and identify possible landmarks by processing images, the second was used to determine the vector measurement from the camera to landmark center positions, and the third was used to estimate the UAV attitude from the previous vectors [20]. It is worth mentioning that the camera must have great stability to perform the desired task, and that any significant and continuous disturbance can affect the final results accuracy.

Beyond guiding the quadrotor on a desired trajectory, a high number of controllers are usually designed to attenuate the load motion, even in the presence of external environmental disturbances. Due to its dynamic and under-actuated system, a cascade controller is commonly chosen for this purpose. A passivity based controller was studied to mitigate the payload disturbances on the quadrotor over a desired flight. It was used not only to control the position of the quadrotor, but also to attenuate its payload oscillation. The passivity-based controller model was decoupled into an inner and outer loop sub-models, where the inner loop stabilised the attitude of the quadrotor, while the outer loop controlled the translational dynamics, including its load dynamics [21].

A cascade control law, based on an uncertainty and disturbance estimator, was designed for a quadrotor with a slung payload. The controller model relied on a combination of two loops, where the outer loop stabilised the quadrotor along a path beyond estimating disturbances, and the inner loop (attitude tracking) was used to control the desired direction of the lift vector. Numerical simulations have shown that the proposed controller stabilised the quadrotor efficiently under different wind disturbances [22].

An Adaptive Sliding Mode Control (ASMC) was studied to verify the UAV flight performance under disturbances and unknown mass. The purpose of the ASMC was to maintain its controller performance, since the UAV presented the ability to pick up and deliver payloads of unknown mass, while they are subjected to disturbances during the flight. The SMC design is often composed of two parts: a continuous

https://doi.org/10.1017/aer.2022.35 Published online by Cambridge University Press

and a discontinuous one. An integral compensation was added in the discontinuous part of the SMC to ensure the sliding motion, even when abrupt changes in the total mass and inertia were addressed. In comparison to the traditional LQR, the proposed strategy gives a better control performance especially during the mass change and release phases [23].

An optimal control model was proposed for a hexarotor that considered different cost functions and various wind loads. Several simulations were conducted using the objective functions such as "minimum effort", "collision-free" and "windy environment". The algorithm based on "modified artificial potential field" was chosen to guide the hexarotor to accomplish safe trajectory tracking as well as to avoid obstacle regions. Experimental tests were also performed to demonstrate the effectiveness of the proposed control approach for hexarotors [24].

It is known that two kinds of attachments are frequently used: (i) a compartment that is fixed on the quadrotor body and (ii) the swing load payload which moves freely on a rope. According to some parameters, such as the UAV transported mass, distance and velocity, one attachment has been chosen from these two attachments mentioned above. Drones are very well known for transportation purposes especially after Amazon announcements of their plans to use them to deliver packages to customers [25], including for their use for health products transportation. The advantages of rapid delivery of vaccines, medication and supplies exactly in the places where they are needed, motivating researchers' efforts to work in the area of drones development.

The feasibility of the UAVs use has been explored in human organ transportation. A commercial drone DJJI M600 Pro was used and a smart cooler was attached directly to the UAV body. In addition, biosensors, vibration sensors, temperature, barometric pressure and altitude measurements sensors were added to the load compartment to provide reliable information regarding the transported organ and the UAV trajectory. Since organ tissues are fragile, they can be deteriorated during the flight by excessive vibrations caused by the quadrotor itself or by continuous external disturbances. Therefore, when an appropriate compartment is attached to the correspondent UAV, it guarantees the best quality of the transported product besides reducing the loss of the organ due to logistic factors [26].

The impact of drone transportation on the insulin quality was also studied. Experiments were conducted to evaluate the insulin quality after its UAV transportation, since it may become unusable in case when an irreversible aggregation forms due to high temperature or vibrations. For these experiments, a commercial drone (DJI Mavic air) including a box of insulin were attached directly to the body of the UAV. Whenever vibrations affect the UAV frame, they could be sent to the payload, since there was a direct connection between the UAV and its payload. Therefore, by understanding the way in which some adverse factors, such as vibrations, external disturbances, abrupt manoeuvers and other conditions may affect both systems, it might increase the chances to choose an appropriate UAV for specific products transportation, as well as to contribute in the design of its robust attachments [27].

This paper investigates a new configuration for a quadrotor type UAV by considering a payload and a flexible attachment system. Dryden continuous gust is also considered during the flight to verify the controller suppression performance and to establish a relationship between both controllers. The main contributions of this paper are: (i) a new dynamic configuration of a quadrotor with a payload using a flexible attachment, (ii) the use of controllers not only to assess the flight performance, as traditionally found in the literature, but also to verify the relative trajectory oscillation influence over the quadrotor dynamics and (iii) the use of Fast Fourier Transform and Performance Indices to evaluate both controllers in different phases of the flight.

This paper is organised in various sections; the Section 2 shows the new dynamic model designed and developed for fragile products transportation, corresponding to a quadrotor with its attached payload model. Two controllers are presented, a Proportional Derivative and a Sliding Mode Controller. Section 3 presents the numerical results obtained by the use of both controllers in mitigating the oscillations occurring between the quadrotor and its load, but also by evaluating the quadrotor performance trajectory under external disturbances. This paper is finalised with concluding remarks presented in Section 4.

https://doi.org/10.1017/aer.2022.35 Published online by Cambridge University Press

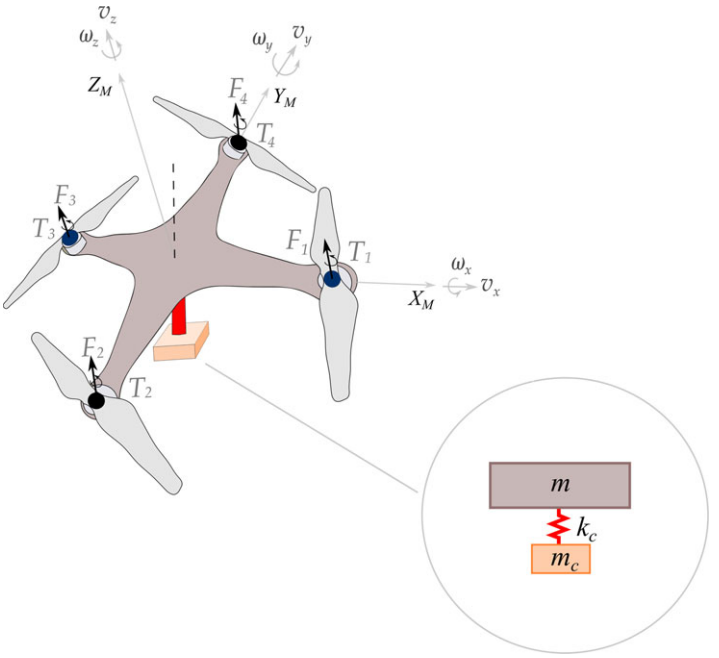

Figure 1. *Schematic illustration of a quadrotor and its proposed attachment.*

2.0 Methodology

The conventional mathematical model of a quadrotor has been described in several Refs. [28–33]. The quadrotor is assumed to be a rigid body, symmetrical around its body-frame origin, with its coordinates axes coinciding with its centre of gravity (CG). The quadrotor is composed of four rotors which are fixed in a cross configuration, and their aerodynamics interactions are neglected. Mathematical modeling has been used to evaluate the effects of vibrations on the payload, which could be a serious challenge to transport safely medical products by the quadrotor.

A payload is attached directly to the quadrotor body and due to the proposed configuration, its motion is assumed to take place only in the vertical direction. Both lateral stiffnesses are larger than the vertical stiffness, such that the lateral relative displacements can be neglected. Figure 1 depicts the coupled system, in which the payload is linked to the quadrotor, and any phenomena that quadrotor undergoes is transmitted directly to its payload. Notice that the quadrotor is assumed to be a rigid body, and for this reason its natural frequencies are higher than the frequency associated to the payload connection.

As shown in Fig. 1, the attachment system consists of a stiffness k_c oriented in the vertical direction, defined in the body-fixed coordinate system (Z_M), in which connects the payload m_c to the quadrotor. The equation of motion of the coupled system is presented in Equation (1):

$$\mathbf{M}_{\eta_c}(\boldsymbol{\eta}_c)\ddot{\boldsymbol{\eta}}_c + \mathbf{C}_{\eta_c}(\boldsymbol{\nu}, \boldsymbol{\eta}_c)\dot{\boldsymbol{\eta}}_c + \mathbf{g}_{\eta_c}(\boldsymbol{\eta}_c) + \mathbf{K}_{\eta_c}(\boldsymbol{\eta}_c)\boldsymbol{\eta}_c = \boldsymbol{\tau}_{\eta_c}(\boldsymbol{\eta}_c) + \mathbf{F}_d \tag{1}$$

where $\mathbf{M}_{\eta_c}(\boldsymbol{\eta}_c)$ is the inertial matrix, $\mathbf{C}_{\eta_c}(\boldsymbol{\nu}, \boldsymbol{\eta}_c)$ represents the Coriolis matrix, $\mathbf{g}_{\eta_c}(\boldsymbol{\eta}_c)$ is the gravitational vector, $\mathbf{K}_{\eta_c}(\boldsymbol{\eta}_c)$ is the stiffness matrix, $\boldsymbol{\tau}_{\eta_c}(\boldsymbol{\eta}_c)$ denotes the control torque, $\mathbf{F}_d$ is the gust vector, and ν is the velocity generalised coordinate in the body-frame. The stiffness matrix $\mathbf{K}_{\eta c}(\boldsymbol{\eta}_c)$ is given by $\mathbf{J}_c\mathbf{M}_c^{-1}\mathbf{K}_c$ as shown in App. A.0 and $\mathbf{K}_c$ is expressed as:

$$\mathbf{K}_c = \begin{bmatrix} \mathbf{0}_{7\times 2} & \mathbf{k}_c & \mathbf{0}_{7\times 3} & -\mathbf{k}_c \end{bmatrix}^T \tag{2}$$

where $\mathbf{k}_c = \{0 \quad 0 \quad k_c \quad 0 \quad 0 \quad 0 \quad -k_c\}^T$ and $\mathbf{0}_{a\times b}$ are zero matrices with a rows and b columns. As already said, the payload moves only in the vertical direction, such that k_x and $k_y >>> k_z$, and the x

https://doi.org/10.1017/aer.2022.35 Published online by Cambridge University Press

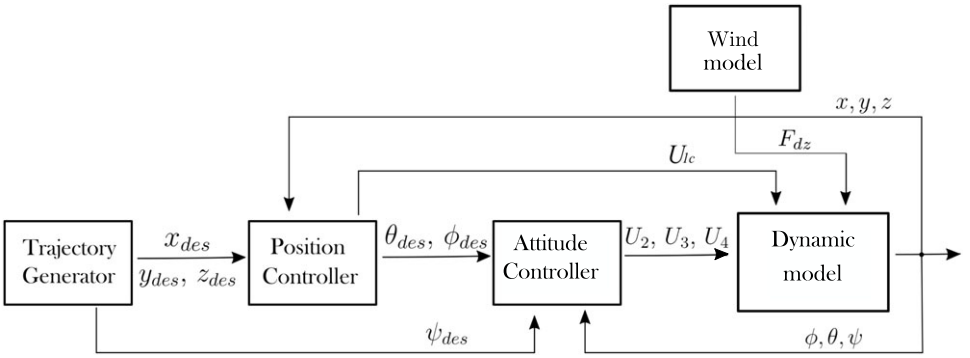

Figure 2. *Control strategy for the quadrotor.*

and y coordinates are assumed to be the same with those of $x = x_c$ and $y = y_c$ (for the quadrotor and its payload, respectively). Therefore, as the lateral displacement can be neglected in the proposed model, the vertical component represents the total significant displacement of the payload. Additionally, $\boldsymbol{\eta}_c$ is the generalised coordinate's vector of the quadrotor in the inertial reference frame and is given by:

$$\boldsymbol{\eta}_c = \begin{Bmatrix} x & y & z & \phi & \theta & \psi & z_c \end{Bmatrix}^T \tag{3}$$

where x,y,z and ϕ, θ, ψ are the positions and orientation angles of the quadrotor, and z_c is the position of the attached mass. The details of the proposed model are found in Appendix A.0, and they emphasise the payload influence on the whole dynamics system.

2.1 Controllers development

The proposed controllers consider four inputs to the dynamic model, such as the vertical altitude z, roll ϕ, pitch θ and yaw ψ angles. The development and comparison of two controllers: Proportional Derivative (PD) and Sliding Mode Control (SMC) is presented in this section. This development aims to achieve not only the UAV trajectory tracking stabilisation, but also to guarantee an attenuation of the relative displacements between the quadrotor and its attached system subjected to external disturbances. These controllers are selected for this study because they are the most used for quadrotor control, as shown in Refs. [11, 12, 34, 35, 37]. The comparison between the SMC and the PD controllers has been made to assess the main contributions of this paper, that consists in the new dynamic configuration and vibration suppression over the quadrotor flight phases.

The trajectory tracking technique is designed using two different loops: the "inner" and "outer" loops. The "outer loop" is related to the Position Controller by giving the input U_{1c} to the dynamic model, and by providing the set of points (ϕ_{des}, θ_{des}) for the "inner loop". The "inner loop" is related to the Attitude Controller, which provides the inputs U_2, U_3 and U_4 to the dynamic model.

In contrast to conventional quadrotors, the position controller U_{1c} requires the combination of the vertical motion equations from the quadrotor with those of the payload output, since the U_{1c} must be able to lift the total mass, as shown in App. C.0. As an under actuated system, the compensation for U_{1c} is then used for the whole controller, since the inputs and outputs for both loops are directly linked. For instance, the pair (ϕ_{des}, θ_{des}) depends on the U_{1c} to be calculated and at the same time is responsible to generate the other inputs U_2 and U_3. Figure 2 represents the cascade control strategy.

The wind model is developed using the Dryden gust methodology applied only in the vertical direction for the quadrotor and its payload, such that the Dryden disturbance is a force defined as $\mathbf{F}_{dz}$. The input control of the dynamic model is calculated using the combination of the inputs U_i ($i = 1, 2, 3, 4$) provided from both loops. Thus, the input control is defined as $\boldsymbol{\tau} = \{0 \;\; 0 \;\; U_{1c} \;\; U_2 \;\; U_3 \;\; U_4 \;\; 0\}^T$.

https://doi.org/10.1017/aer.2022.35 Published online by Cambridge University Press

2.1.1 Proportional Derivative (PD) control

The Proportional Derivative (PD) control design is described in this sub-section. It is worth mentioning again that the payload is directly attached to the quadrotor frame, and this connection is assumed to link the quadrotor to its payload. Therefore, any disturbance (gust, vibration) affecting the quadrotor may also affect the payload, i.e. the motion of the payload z_c is directly related to z. In this sense, as shown in App. C.0, the altitude controller requires a combination of the quadrotor with payload motions in order to accomplish the desired vertical trajectory. The modified control law in the z direction is defined by the total thrust of motors:

$$U_{1c} = \tilde{m}(g + r_z)/c\phi c\theta \tag{4}$$

where $c(.)$ is the cosine function, and r_z can be written as $r_z = k_{pz}(z_{des} - z) + k_{dz}(\dot{z}_{des} - \dot{z})$. In addition, z_{des} and z are the desired and current altitudes, $\dot{z}_{des}$ and $\dot{z}$ are their time derivatives, and k_{pz} and k_{dz} are the proportional and derivative gains of the controller, respectively.

For a regular quadrotor, $\tilde{m}$ is defined only for its mass m (as widely seen in literature [36]). However, the new quadrotor can carry out different payload, and the heavier the extra weight added to the quadrotor is, the more its flight altitude is affected. To compensate for the extra weight added to the system, $\tilde{m}$ is defined by $m + m_c$.

In the inner loop, two phases are required to properly control the quadrotor. Firstly, the total thrust needs to be calculated by use of Equation (4). Secondly, to ensure the motion of the quadrotor in the (x,y) planes, the desired roll and pitch angles $(\phi_{des}, \theta_{des})$ are generated through their expressions, as given in [37]:

$$\phi_{des} = sin^{-1}(s\psi U_x - c\psi U_y) \quad \theta_{des} = sin^{-1}[(U_x - s\psi s\phi)/(c\psi c\phi)], \tag{5}$$

where the virtual inputs U_x and U_y are defined as follows:

$$U_x = (r_x\tilde{m})/U_{1c} \quad U_y = (r_y\tilde{m})/U_{1c}, \tag{6}$$

Similar to r_z, in the x and y planes, $r_x = k_{px}(x_{des} - x) + k_{dx}(\dot{x}_{des} - \dot{x})$ and $r_y = k_{py}(y_{des} - y) + k_{dy}(\dot{y}_{des} - \dot{y})$. Moreover, as the inner loop is fully controllable, the torques are applied at roll, pitch and yaw angles (ϕ, θ, ψ). After linearising and applying the necessary simplifications, the rotational equations can be defined as: $U_2 = (I_{xx} + \Delta I_{xx})\ddot{\phi}$, $U_3 = (I_{yy} + \Delta I_{yy})\ddot{\theta}$, and $U_4 = (I_{zz} + \Delta I_{zz})\ddot{\psi}$. Thus, the inputs of the simplified rotational proposed controller are defined as follows:

$$\begin{aligned} U_2 &= k_{p\phi}(\phi_{des} - \phi) + k_{d\phi}(\dot{\phi}_{des} - \dot{\phi}) \\ U_3 &= k_{p\theta}(\theta_{des} - \theta) + k_{d\theta}(\dot{\theta}_{des} - \dot{\theta}) \\ U_4 &= k_{p\psi}(\psi_{des} - \psi) + k_{d\psi}(\dot{\psi}_{des} - \dot{\psi}), \end{aligned} \tag{7}$$

where k_{pi} and k_{di} are the proportional and derivative gains defined for the "inner loop", where $(i = \phi, \theta, \psi)$.

2.1.2 Sliding mode control (SMC)

This sub-section presents the design of a Sliding Mode Control (SMC) strategy. The combination between the position and the velocity tracking errors of state variables allows for the development of a second order Sliding Mode Control (SMC). The proposed controller system is divided into two sub-systems: (i) a fully actuated sub-system ($\ddot{z}$ and $\ddot{\psi}$) and (ii) an under actuated subsystem ($\ddot{x}$, $\ddot{y}$, $\ddot{\phi}$ and $\ddot{\theta}$). The fully actuated controller ensures the convergence of the current variables $[z, \psi]$ to the desired ones $[z_{des}, \psi_{des}]$. For the vertical motion variable z, a sliding surface equation determines the dynamics of the system by using [38]:

$$s_z = \lambda_z(z_{des} - z) + (\dot{z}_{des} - \dot{z}), \tag{8}$$

where λ_z is a "tuning" parameter associated with the "closed loop bandwidth". Furthermore, the derivative of s_z is calculated with respect to time such as $\dot{s}_z = \lambda_z(\dot{z}_{des} - \dot{z}) + (\ddot{z}_{des} - \ddot{z})$.

https://doi.org/10.1017/aer.2022.35 Published online by Cambridge University Press

In fact, the time derivative s_i can also be defined by using a discontinuous state function to enforce the proposed controller on the surface, such that $\dot{s}_i = -\epsilon_i sat(s_i) - \eta_i s_i$, where ϵ_i and η_i are the sliding surface exponential approach coefficients, and sat(.) indicates the saturated function. By combining the time derivative ($\dot{s}_z$), the state function ($\dot{s}_i$) and the equations of motion in the z and z_c directions (as seen in [16]) the corresponding control law input is defined as

$$U_{1c} = \frac{\tilde{m}}{c\theta c\phi}(\epsilon_z sat(s_z) + \eta_z s_z + \lambda_z(\dot{e}_z) + \ddot{z}_{des} + g), \tag{9}$$

where $\dot{e}_z$ is the difference between the desired and the calculated state variables ($\dot{z}_d$ - $\dot{z}$), and $sat(s_i)$ is the saturated function used to alleviate the effect of chattering on the actuators, as shown in [39]:

$$sat(s_i) = \frac{s_i}{|s_i| + \gamma} \tag{10}$$

where γ is the parameter used to define the "transition bandwidth" (which can reduce the chattering effect on the actuators). Likewise to the Proportional Derivative, in the "inner loop", two phases are required to control the quadrotor. First, the total thrust must be calculated with the Equation (9). Second, to enable the motion of the quadrotor in the (x,y) plane, the desired roll and pitch angles (ϕ_{des}, θ_{des}) are generated through two virtual inputs. These inputs are two dependent position states (x, y) for the SMC, and each position state requires virtual inputs to obtain the under-actuated controller parameters. Therefore, the desired angles of roll and pitch for designing the attitude control are obtained with Equation (11) [40]:

$$\phi_{des} = sin^{-1}(u_x s\psi - u_y c\psi) \qquad \theta_{des} = sin^{-1}\left(\frac{u_x c\psi + u_y s\psi}{c\psi}\right) \tag{11}$$

where u_x and u_y are defined by $u_x = \frac{\tilde{m}}{U_{1c}}(\ddot{x}_{des} + \lambda_x \dot{e}_x + \eta_x s_x + \epsilon_x sat(s_x))$ and $u_y = \frac{\tilde{m}}{U_{1c}}(\ddot{y}_{des} + \lambda_y \dot{e}_y + \eta_y s_y + \epsilon_y sat(s_y))$, where λ_x, λ_y, η_x, η_y, ϵ_x and ϵ_y are positive real constants. Similarly, U_2, U_3 and U_4 are obtained following the same steps as the ones mentioned previously for U_{1c}, therefore they are obtained with next Equation (12):

$$\begin{aligned}
U_2 &= \frac{I_{xx} + \Delta I_{xx}}{l}(\ddot{\phi}_{des} + \lambda_\phi \dot{e}_\phi + \eta_\phi s_\phi + \epsilon_\phi sat(s_\phi)) - [(I_{yy} + \Delta I_{yy}) - (I_{zz} + \Delta I_{zz})]l\dot{\theta}\dot{\psi} \\
U_3 &= \frac{I_{yy} + \Delta I_{yy}}{l}(\ddot{\theta}_{des} + \lambda_\theta \dot{e}_\theta + \eta_\theta s_\theta + \epsilon_\theta sat(s_\theta)) - [(I_{zz} + \Delta I_{zz}) - (I_{xx} + \Delta I_{xx})]l\dot{\phi}\dot{\psi} \\
U_4 &= (I_{zz} + \Delta I_{zz})(\ddot{\psi}_{des} + \lambda_\psi(\dot{e}_\psi) + \eta_\psi s_\psi + \epsilon_\psi sat(s_\psi)) - [(I_{xx} + \Delta I_{xx}) \\
&\quad -(I_{yy} + \Delta I_{yy})]\dot{\theta}\dot{\phi}
\end{aligned} \tag{12}$$

where λ_ϕ, λ_θ, λ_ψ, ϵ_ϕ, ϵ_θ, ϵ_ψ, η_ϕ, η_θ and η_ψ are also positive real constant parameters.

2.2 Performance indices

Performance indices are employed to evaluate both controllers in different phases of flight, as well as their relative oscillations. A system exhibits its best performance when the controller parameters are adjusted to reach the minimum values of the performance indices [41]. The first index is called the "Integral of the Absolute magnitude of the Error" (IAE), which is used in numerical simulations and is defined with the next Equation (13):

$$IAE = \int_0^T |e_o(t)|dt, \tag{13}$$

where $|e_o(t)|$ is the absolute oscillation error, and is given by the difference between the quadrotor and the load displacements ($|z_c - z|$). T is the final time of each flight phase (since the trajectory is divided into three phases: taking-off, cruise and landing). Another proposed performance index is called the

https://doi.org/10.1017/aer.2022.35 Published online by Cambridge University Press

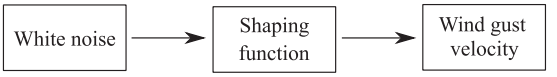

Figure 3. *Process for generating Dryden wind velocity model.*

"Integral of Time multiplied by the Absolute Error" (ITAE), that is designed to reduce the errors at the beginning of the signal, as well as to obtain the steady-state error:

$$ITAE = \int_0^T t|e_o(t)|dt, \tag{14}$$

where t is the simulation time. Other performance indices can be found in Ref. [42].

2.3 Dryden continuous gust

Turbulence, also called wind gust, is described as a brief change of wind velocity caused by atmospheric pressure and temperature. Therefore, a realistic model is required to evaluate its effects on a UAV [43], and the Dryden and Von Kármán are two of the most common models used to study the wind effects on UAVs. The expression of the Dryden Power Spectral Density (PSD) defining the turbulence velocity in the vertical direction is represented by [44, 45]:

$$\Phi_z(\Omega) = \sigma_z^2 \frac{L_z}{\pi} \frac{1 + 3(L_z\Omega)^2}{(1 + (L_z\Omega)^2)^2} \tag{15}$$

Fundamentally, a Power Spectral Density (PSD) function is parameterised using the turbulence scale length (L_z) and standard deviations (or turbulence intensities), defined as σ_z. For lower-altitudes than 60m, these parameters are given by $L_z = h$ and $\sigma_z = 0.1w_{ws}$, where w_{ws} denotes the mean wind speed and h is the flying altitude of the quadrotor. Then, in order to generate the wind gust velocity, a white noise signal is filtered through a shaping function, as shown on Fig. 3.

The relationship between the Power Spectral Density (PSD) and the transfer function is given by [46]:

$$\Phi_i(\Omega) = |G(j\omega)^2| = G^*(j\omega)G(j\omega), \tag{16}$$

where $*$ indicates the complex conjugate of the transfer function. The transfer function of the shaping filter can be obtained by decomposing the PSD, as seen in Equation (16), and in [47]:

$$G_z(s) = \frac{v_{z_d(s)}}{\eta_z(s)} = \sigma_z \sqrt{\frac{L_z}{\pi V}} \frac{1 + \frac{\sqrt{3}L_z}{V}s}{\left(1 + \frac{L_z}{V}s\right)^2}, \tag{17}$$

where η_z denotes the white Gaussian noise in the frequency domain. V is the wind velocity and s is the Laplace variable (which can be replaced by $j\omega$ in order to solve the Equation (17)). Therefore, after finding the wind velocity v_{z_d} and converting it into time, the wind gust velocity in the inertial reference can be represented as $v_{wz} = \bar{v}_{wz} + v_{z_d}$, where $\bar{v}_{wz}$ denotes the mean wind velocity in the z direction. Finally, the Dryden disturbance F_{dz}, that acts on the UAV during a flight, is defined as:

$$F_{dz} = -\frac{1}{2}\rho C_{dz} A_z (\dot{z} - v_{wz})^2 sgn(\dot{z} - v_{wz}), \tag{18}$$

where ρ is the air density, C_{dz} is the drag coefficient, $sgn(.)$ denotes the sign function, A_z is the area projected by the UAV and $\dot{z}$ is the velocity along the z axis, respectively. The same steps are required to design the Dryden disturbance force that acts on the payload, switching only the velocity of the payload $\dot{z}_c$ instead of $\dot{z}$. The forces and Dryden components along the (x, y) axes are detailed in Appendix B.0.

https://doi.org/10.1017/aer.2022.35 Published online by Cambridge University Press

Table 1. *Parameters of the quadrotor model*

Parameter	Value	Unit
m	2.2	kg
l	0.1725	m
g	9.81	m/s^2
I_{xx}	0.0167	kgm^2
I_{yy}	0.0167	kgm^2
I_{zz}	0.0231	kgm^2

Table 2. *Controller gains computed for the PD and SMC methodologies*

Method	Parameters	Value	Parameters	Value
PD	k_{px}, k_{py}, k_{pz}	1.50, 1.60, 1.50	k_{dx}, k_{dy}, k_{dz}	1.80, 1.80, 2.00
	$k_{p\phi}$, $k_{p\theta}$, $k_{p\psi}$	0.40, 0.70, 1.00	$k_{d\phi}$, $k_{d\theta}$, $k_{d\psi}$	0.10, 0.05, 0.05
SMC	ϵ_x, ϵ_y, ϵ_z,	2.20, 1.80, 1.80	ϵ_ϕ, ϵ_θ, ϵ_ψ,	1.50, 1.10, 1.10
	λ_x, λ_y, λ_z	3.00, 3.20, 3.20	λ_ϕ, λ_θ, λ_ψ	1.50, 1.50, 1.50
	η_x, η_y, η_z	0.40, 0.40, 0.40	η_ϕ, η_θ, η_ψ, γ	0.04, 0.04, 0.04, 0.20

3.0 Results and discussion

The dynamic parameters of the quadrotor with an attached payload are presented in Table 1 in terms of their physical and geometrical properties. The initial yaw angle is considered as $\psi = 0.5$rad, while the other desired initial states $(x, y, z, \phi, \theta, \psi)$ are defined as equal to zero. The controller gains of both controllers (PD and SMC) are listed in Table 2. The PD gains were initially selected according to their values previously employed in Ref. [37], and the new SMC gains were chosen based on the pole placement method. The defining step of the controller gains is very important to obtain a successful controller design. These following results are obtained by integrating Equation (1) in time domain, using Matlab software. The Fourth Order Runge-Kutta algorithm was employed with time step 2×10^{-4}s.

The flight trajectory used to evaluate the relative trajectory oscillation is shown in Fig. 4, and this trajectory is built for three phases: transient P_1, cruise P_2 and landing P_3. The first phase occurs between the beginning of a flight and the time when the quadrotor reaches the desired altitude (in the absence of transient effects). The second phase represents the cruise path, where the quadrotor flies horizontally at the same altitude, while the third phase covers the descent until the quadrotor lands on the ground[1].

It is worth mentioning that the controller has no direct actuation on the payload, allowing the payload to move freely in the vertical direction. On the other hand, the controller acts directly on the quadrotor motion, by orientating its flight on a pre-defined trajectory and suppressing residual oscillations. Therefore, due to the direct impact of the controller, the payload displacements are larger than the quadrotor, and influenced by the attachment stiffness k_c.

The relative trajectory oscillation is defined by the difference between the vertical displacement of the payload and the vertical displacement of the quadrotor, therefore it is denoted by $z - z_c$. In the beginning of the flight, when a transient effect occurs, the oscillations can be attenuated differently by using both controllers (SMC and PD). Figure 5 shows the oscillation of each controller during the first phase P_1. The relative trajectory oscillation between the quadrotor and its payload can then be calculated with a Fast Fourier Transform (FFT), denoted by $|Z|$.

As seen in Fig. 5, the SMC presents better performance compared to that of the PD, as the transient phase has less effect the SMC case. Figure 6 shows the frequency spectrum of the oscillation, for which

[1] For the proposed mathematical modeling, the distance between the payload and quadrotor is neglected.

https://doi.org/10.1017/aer.2022.35 Published online by Cambridge University Press

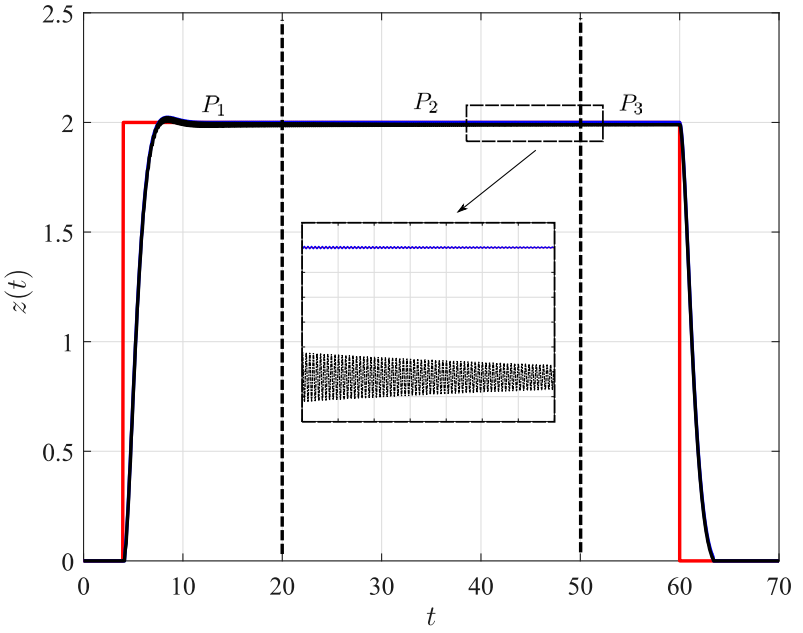

Figure 4. *Trajectory of the quadrotor in the z direction, showing the desired trajectory (solid red line), the quadrotor path (solid blue line) and the payload displacement (dashed black line).*

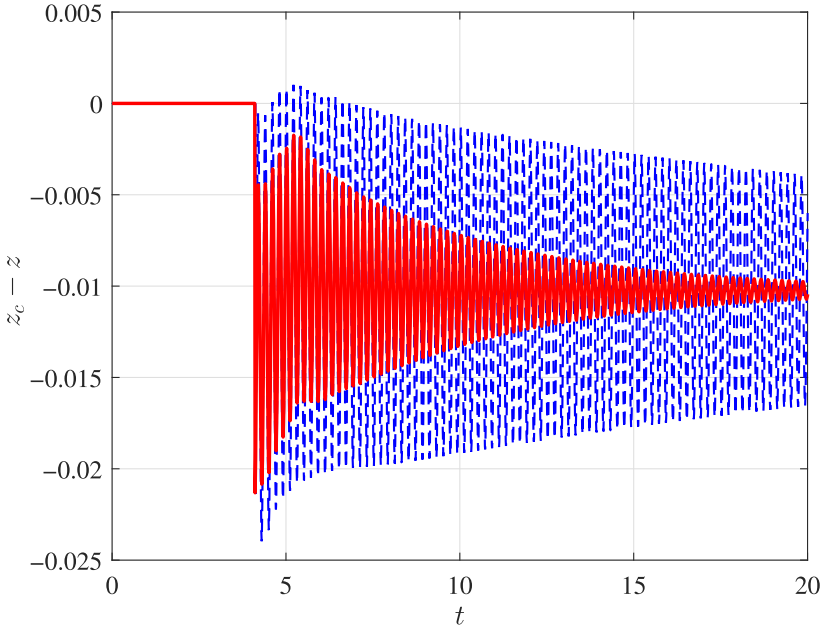

Figure 5. *Relative trajectory oscillation in the transient phase, for the PD (dashed blue line), and the SMC (solid red line).*

https://doi.org/10.1017/aer.2022.35 Published online by Cambridge University Press

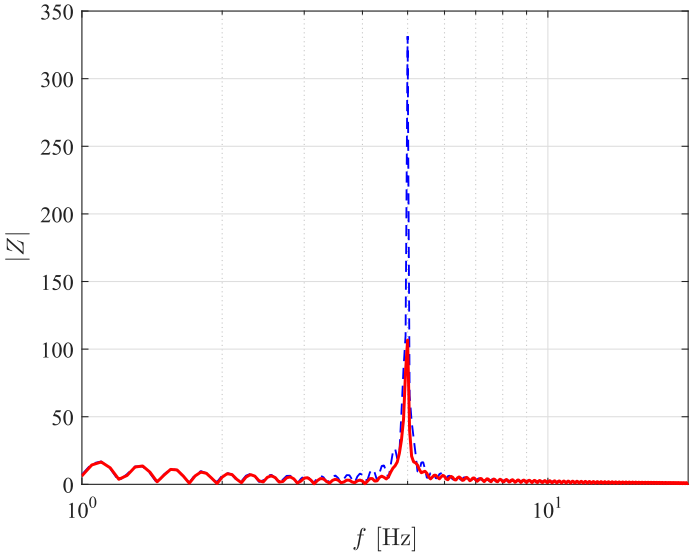

Figure 6. *Frequency spectrum of the relative trajectory oscillation at P_1, for the PD (dashed blue line), and the SMC (solid red line).*

the SMC amplitude peak is approximately 35% of the PD. Notice that the payload displacement z_c is different when comparing the SMC and the PD controllers performance. The SMC laws guarantee a better adherence to the quadrotor trajectory, and therefore higher oscillation suppression as results in comparison to the PD performance results.

Both controllers are used to evaluate the performance of a quadrotor when is subjected to an external disturbance during the second phase P_2. The proposed controllers are designed to reduce the relative trajectory oscillation produced by the coupling of a quadrotor with its attached mass.

When a UAV is subjected to the external disturbances, its trajectory is suddenly changed, and depending on the coupling parameters adopted, the relative displacement can be either enhanced or reduced. Thereby, the controllers must not only stabilise the tracking, but they should also guarantee an attenuation of the oscillations. Figure 7 shows the effect of an external disturbance during the second (cruise) phase P_2 for both controllers. The difference in the vertical direction of the quadrotor and its payload is due to the physical distance of the proposed attachment. The payload is translated vertically below from the CoG of the quadrotor, in order to allow the payload to move freely in this respective direction.

In the absence of external disturbance, the signal has its main impact only for a specific frequency, while in the presence of external disturbance, the response is affected during a range of frequencies, as seen in Fig. 8. Moreover, the peak is smaller and the band is narrower than when a disturbance impacts on the trajectory. It can be seen in Fig. 7 that the SMC reduces the oscillation more than the PD. Especially at the time when a disturbance is applied to the system [25–40]s, not only the peak amplitude calculated with the SMC is smaller than that calculated with the PD, but the time required for the system to return to a minimum oscillation is also reduced.

The SMC is able to reduce the gust effect more than the PD mainly because its formulation allows one to consider boundary uncertainties. Note that a discontinuous state function ($\dot{s}_i = -\epsilon_i sat(s_i) - \eta_i s_i$) was used to enforce the proposed controller on the surface, which improves the SMC with respect to the PD in terms of noise reduction and trajectory adherence. This approach allowed the quadrotor to follow smoothly its desired path, and therefore to ensure lower effects on its payload performance. Figure 8

https://doi.org/10.1017/aer.2022.35 Published online by Cambridge University Press

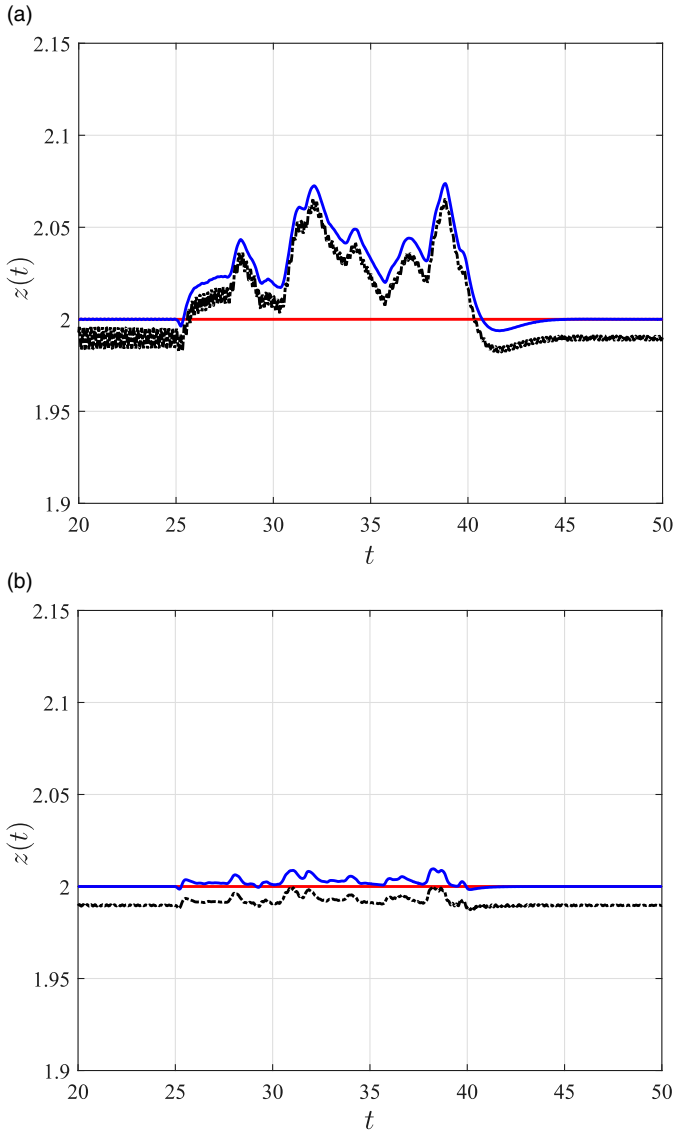

Figure 7. *Trajectory affected by a vertical Dryden wind disturbance using: a) the PD, and b) the SMC, showing the desired trajectory (solid red line), the quadrotor (solid blue line) and the payload displacement (dashed black line).*

illustrates the presence and absence of an external disturbance. Figure 9 shows the relative trajectory oscillation between the quadrotor and the payload during the second phase P_2.

Likewise, by applying the Fast Fourier Transform (FFT) to the signal $(z_c - z)$, it can be shown that the peak calculated with the SMC is around eight times smaller than that found by using the PD. Figure 10 shows the frequency spectrum when an external disturbance is applied on the quadrotor and its attached system during the cruise phase.

In the last phase of landing (P_3), the controllers can attenuate the relative trajectory oscillation, however in contrast to the other two phases, the SMC presents a slight increase of oscillation amplitudes

https://doi.org/10.1017/aer.2022.35 Published online by Cambridge University Press

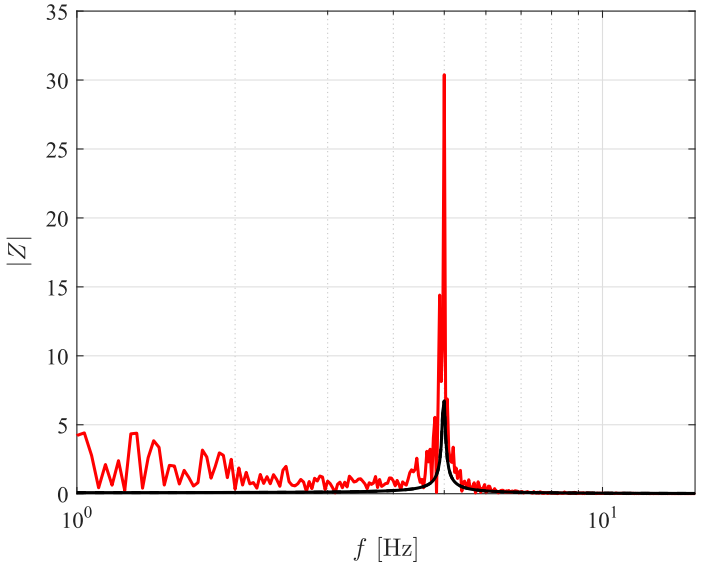

Figure 8. *Frequency spectrum of the relative trajectory oscillation during the cruise phase P_2, that shows the presence of disturbance (solid red line), and the absence of disturbance (solid black line).*

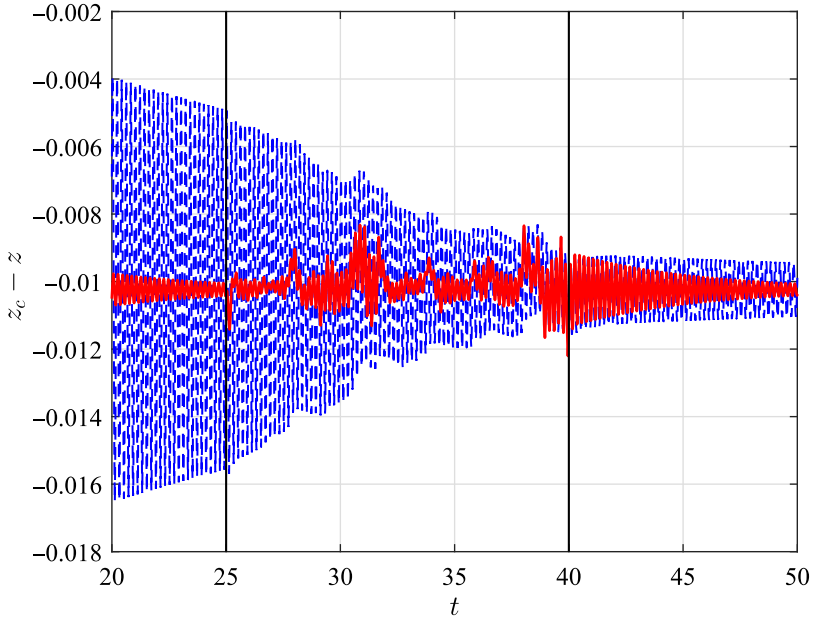

Figure 9. *Relative trajectory oscillation in the second (cruise) phase, for the PD (dashed blue line), the SMC (solid red line), and and the boundaries of the external disturbance (solid black lines).*

https://doi.org/10.1017/aer.2022.35 Published online by Cambridge University Press

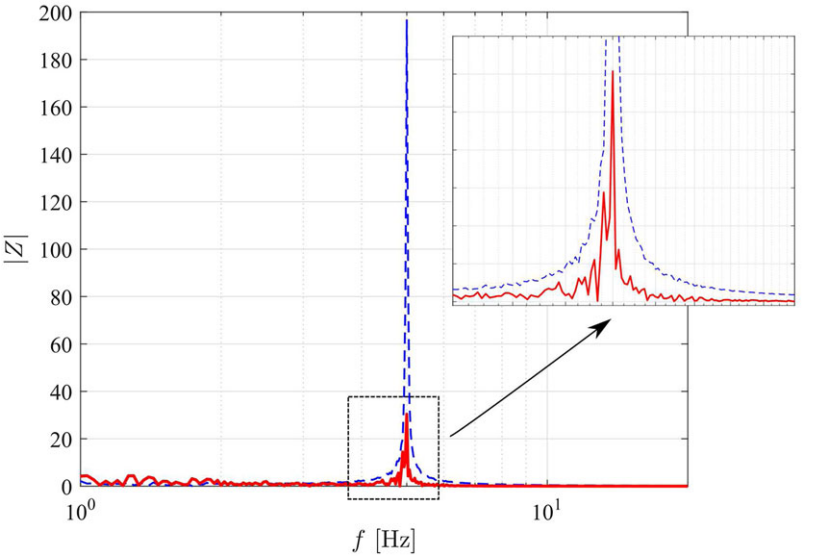

Figure 10. *Frequency spectrum of the relative trajectory oscillation during the second phase P_2, obtained with the PD (dashed blue line), and the SMC (solid red line).*

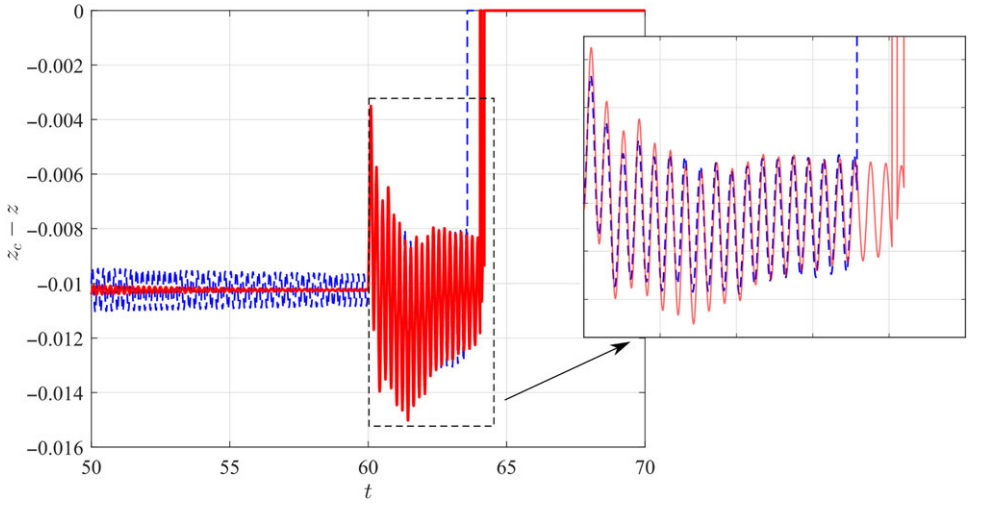

Figure 11. *Relative trajectory oscillation in the landing phase, for the PD (dashed blue line), and the SMC (solid red line).*

compared to the PD when the quadrotor begins the landing process [60–64]s. On the other hand, when the analysis covers the whole P_3 phase [50–70]s, the SMC still gives a better performance than the PD. Figure 11 shows the relative trajectory oscillations when a quadrotor is in the landing process, while Fig. 12 presents the frequency spectrum of the signal.

To compare the performance indices of the two controllers, a percentage parameter can be defined as $P_{pi} = 100\frac{P_{SMC}}{P_{PD}}$, where P_{pi} is the percentage of the performance index (*IAE* and *ITAE*), defined in Section 2.2), P_{SMC} is the index calculated at each phase for the Sliding Mode Control and P_{PD} is the

https://doi.org/10.1017/aer.2022.35 Published online by Cambridge University Press

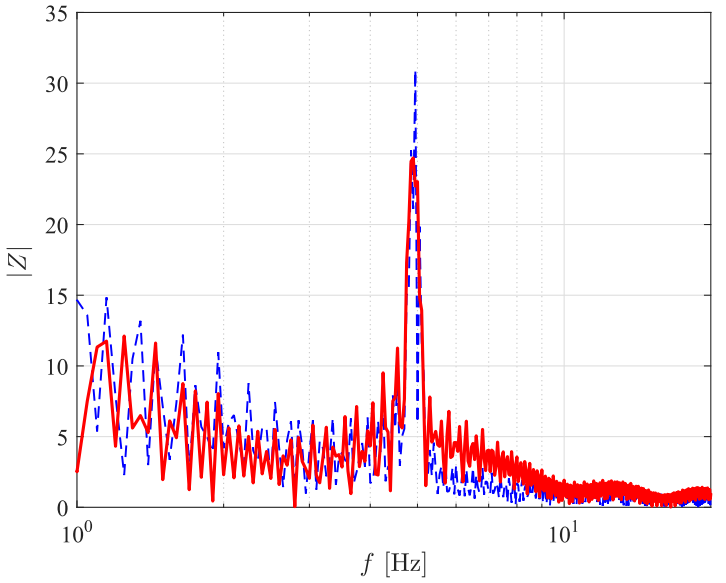

Figure 12. *Frequency spectrum of the relative trajectory oscillation during phase P_3, for the PD (dashed blue line), and the SMC (solid red line).*

index calculated by the Proportional Derivative. Table 3 shows the performance indices calculated for each flight phase.

Based on the Table 3 all performance indices percentages show an advantage for using the SMC rather than the PD (since all percentage of performance indices are lower than 100%, thus they indicate a higher values of P_{PD} than the P_{SMC} values). For instance, by considering the P_{IAE} at the transient phase, the SMC requires only 35.40% of the energy spent by the PD. In addition, when an external disturbance is added to the dynamic system during the cruise phase P_2, a more significant reduction can be observed, since the P_{SMC} represents only 11.38% of the energy required by the P_{PD}. Thereby, when analysing the results obtained for the third phase, the SMC shows a better performance than the PD (with smaller oscillation amplitude, around 49% less interference with the quadrotor and on-board loads dynamics).

Therefore, the SMC controller ensures a more robust stabilisation of the relative trajectory oscillation than PD. Following several tests, as described in [48], it was found that the take-off and landing phases have a significant influence on the flight, reinforcing the importance to study them individually. Thereby the highest oscillation amplitudes are depicted during the P_1 and P_3 phases, as shown in Figs 5 and 11, respectively. Figures 13 and 14 show the relationship between the natural frequency and its highest peak reached by the relative displacement during the first and third phases, respectively.

The A_m term refers to the maximum amplitude reached by the quadrotor. Without changing its controller performance (by switching the gains, propellers velocities or other parameters), different structural parameters, such as stiffness can be chosen with the aim to obtain a lower maximum amplitude. As shown in Fig. 13, the peak of oscillation can thus be significantly reduced depending on the analysed range of frequencies. In addition as shown previously, the SMC gives a better reduction of relative displacements than the PD during the first (transient) phase, which can clearly be observed by the marker position ($*$, $+$) on Fig. 14. Similarly, in the third phase, the maximum amplitude decreases with the increase of the natural frequency (ω_r).

https://doi.org/10.1017/aer.2022.35 Published online by Cambridge University Press

Table 3. *Performance indices [%] for the controllers during three trajectory phases*

Disturbance Position Index	Transient Phase P_1	Cruise Phase P_2	Landing Phase P_3
P_{IAE}	35.40%	11.38%	48.25%
P_{ITAE}	26.73%	13.76%	49.51%

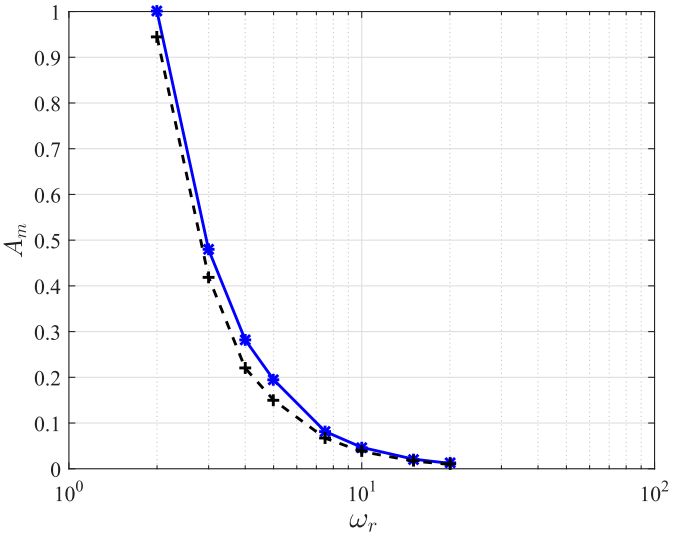

Figure 13. *Maximum amplitude reached by the quadrotor during the take-off phase, for the PD (−∗) and the SMC (- - +).*

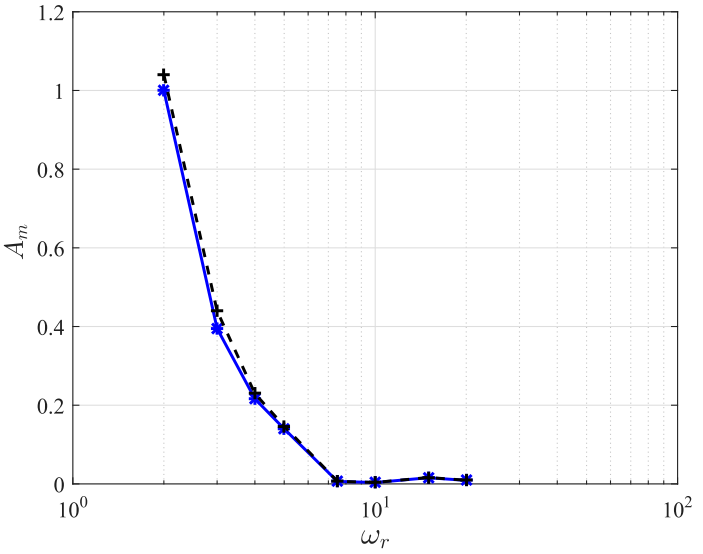

Figure 14. *Maximum amplitude reached by the quadrotor during the landing phase, for the PD (−∗) and the SMC (- - +).*

https://doi.org/10.1017/aer.2022.35 Published online by Cambridge University Press

4.0 Final remarks

This paper investigates the dynamics of a quadrotor with a vibrating payload. The attachment system is composed by a stiffness and an attached mass, which ensures the payload to oscillate only vertically. Two controllers were used to investigate the relative trajectory oscillation between the quadrotor and the payload, as well as the quadrotor performance under external winds disturbances. The proposed strategy allows to compare both controllers (SMC and PD) results in different flight phases and to understand the impact of external disturbances, and manoeuvers on the quadrotor flight. The Sliding Mode Controller has a fast response to fit to the trajectory, especially to compare its performance to the Proportional Derivative (PD). The SMC's faster convergence to the desired point in space is related to its robust control law even under uncertainty parameters (such as external disturbance), which guides and fits strongly the quadrotor trajectory on its proposed path.

In addition, to establish a performance metrics, the Fast Fourier Transform "FFT" of the relative trajectory oscillation, between the quadrotor and its payload, was evaluated to verify how the frequency range impacted the system. It was shown that in the presence of external disturbances, the quadrotor was affected by a larger frequency spectrum and had a significant effect on its energy (represented by its peak) in comparison to its behaviour in the absence of external disturbances. When analysing the effects of external disturbances (during the second phase P_2), the SMC clearly gives a better performance than the PD. The performance indices were also calculated to measure the trajectory tracking of the quadrotor and the payload. The performance index is about ten times smaller (for the SMC than for the PD) indicating the lower relative trajectory oscillations. The use of a more robust controller can thus improve not only the trajectory tracking but can also reduce the vibration sent to the payload.

The recommendations for future works include the analysis of the controller performance, by considering an external disturbance in different phases of a flight, such as take-off, landing or sudden change of altitude. The understanding of the undesired vibration influence on the whole flight is also an interesting topic for further investigations in this field.

Acknowledgments. The first author would like to thanks to the Brazilian Coordination for the Improvement of Higher Education Personnel (CAPES) - Finance Code 001 for his scholarship. The second author thanks to the NSERC for the Canada Research Chair Holder Tier 1 in Aircraft Modeling and Simulation Technologies Program. The third author gives special thanks to the National Council for Scientific and Technological Development (CNPq) Grant no. 429963/2016-5 for its financial support.

Declaration of conflicting interests. The authors declared no potential conflicts of interest with respect to the research, authorship, and/or publication of this paper.

References

[1] Mohammed, F., Idries, A., Mohamed, N., Jaroodi, J. and Jawhar, I. Uavs for Smart Cities: Opportunities and Challenges, *International Conference on Unmanned Aircraft Systems (ICUAS)*, pp 267–273, 2014.

[2] Heintz, F., Rudol, P. and Doherty, P. From images to traffic behavior - A UAV tracking and monitoring application, 2007 *10th International Conference on Information Fusion*, pp 1–8, 2007.

[3] Dufek, J., Traore, S., Swanson, C., Fipps, G. and Murphy, R. Preventing irrigation canal breaches using small unmanned aerial system with multispectral payload, 2019 *IEEE International Symposium on Safety, Security, and Rescue Robotics (SSRR)*, pp 133–138, 2019.

[4] Ghamry, K.A., Kamel, M.A. and Zhang, Y. Cooperative forest monitoring and fire detection using a team of UAVs-UGVs, IEEE, 2016 *International Conference on Unmanned Aircraft Systems (ICUAS)*, pp 1206–1211, 2016.

[5] Lin, Z., Liu, H.H.T. and Wotton, M. Kalman Filter-based large-scale wildfire monitoring with a system of UAVs, *IEEE Trans Indus Electron*, 2019, **66**, (1), pp 606–615.

[6] Paredes, J.A., Acevedo, J., Villalta, J. and Furukawa, R. Quadrotor Design for medicine transportation in the peruvian amazon rainforest, 2016 *IEEE XXIII International Congress on Electronics, Electrical Engineering and Computing (INTERCON)*, pp 1–6, 2016.

[7] Ahmad, F., Kumar, P. and Patil, P.P. Modeling and simulation of a quadrotor with altitude and attitude control, *Nonlinear Stud.*, 2018, **25**, (2).

[8] Oubbati, O.S., Chaib, N., Lakas, A, Lorenz, P. and Rachedi, A. UAV-assisted supporting services connectivity in urban vanets, *IEEE Trans Vehicul. Technol, 2019*, **68**, (4), 3944–3951.

[9] Ackerman, E. and Koziol, M. The blood is here: Zipline's medical delivery drones are changing the game in Rwanda, *IIEEE Spectrum*, 2019, **56**, (5), pp 24–31.

https://doi.org/10.1017/aer.2022.35 Published online by Cambridge University Press

[10] Kim, J.,Gadsden, S.A. and Wilkerson, S.A.A. Comprehensive survey of control strategies for autonomous quadrotors, *Canadian J Electr Comput Eng*, 2020, **43**, (1), pp 3–16.
[11] Zuniga, N.S., Munoz, F., Marquez, M.A., Espinoza, E.S. and Carillo, L.R.G. Load transportation using single and multiple quadrotor aerial vehicles with swing load attenuation, 2018 *International Conference on Unmanned Aircraft Systems (ICUAS)*, pp 269–278, 2018.
[12] Nascimento, T.P. and Saska, M. Position and attitude control of multi-rotor aerial vehicles: A survey, *Ann Rev Cont*, 2019.
[13] Lee, B.Y., Lee, H.I., Yoo, D.W., Moon, G.H., Lee, D.Y., Kim, Y.Y. and ahk, M.J. Study on payload stabilisation method with the slung-load transportation system using a quad-rotor, 2015 *European Control Conference (ECC)*, pp 2097–2102, 2015.
[14] Zhang, M. and Liu, H.H. Tracking a moving target by a fixed-wing UAV based on sliding mode control, *AIAA Guidance, Navigation, and Control (GNC) Conference*, pp 1–10, 2013.
[15] Yang, S. and Xian, B. Robust control design for the quadrotor UAV with a suspended payload, *IEEE 8th Annual International Conference on CYBER Technology in Automation, Control, and Intelligent Systems (CYBER)*, pp 469–473, 2018.
[16] Elhennawy, A.M. and Habib, M.K. Nonlinear robust control of a quadrotor: Implementation and evaluation, *IECON* 2018 - *44th Annual Conference of the IEEE Industrial Electronics Society*, pp 3782–3787, 2018.
[17] Ricardo, Jr., A.R., Santos, D.A. and Oliveira, T.R. Attitude tracking control for a quadrotor aerial robot using adaptive sliding modes, *Proceedings of the XLI Ibero-Latin-American Congress on Computational Methods in Engineering*, pp 1–7, 2020.
[18] Silva, A.L. and Santos, D.A. Fast nonsingular terminal sliding mode flight control for multirotor aerial vehicles, *IEEE Trans Aerospace Electron Syst*, 2020, **56**, (6), pp 4288–4299.
[19] Zhong, Y. et al. Robust actuator fault detection and diagnosis for a quadrotor UAV with external disturbances, *IEEE Access*, 2018, **6**, pp 48169–48180.
[20] Santos, D.A. and Gonçalves, P.F. Attitude determination of multirotor aerial vehicles using camera vector measurements, *J Intell Robot Syst.*, 2017, **86**, (1), pp 139–149.
[21] Godbole, A.R. and Subbarao, K. Mathematical modeling and control of an unmanned aerial system with a cable suspended payload, 2018 *IEEE 14th International Conference on Control and Automation (ICCA)*, 2018, pp 570–575.
[22] Qian, L. and Liu, H.H.T. Path-following control of a quadrotor UAV with a cable-suspended payload under wind disturbances, *IEEE Trans Ind Electron*, 2020, **67**, (3), pp 2021–2029.
[23] Wang, B., Mu, L. and Zhang, Y. Adaptive robust control of quadrotor helicopter towards payload transportation applications, *Proceedings of the 36th Chinese Control Conference*, pp 1–6, 2017.
[24] Heidari, H. and Saska, M. Collision-free trajectory planning of multi-rotor UAVs in a wind condition based on modified potential field, *Mech Mach Theory*, 2021, **156**, pp 104–140.
[25] Koiwanit, J. Analysis of environmental impacts of drone delivery on an online shopping system, *Adv Clim Change Res*, 2018, **9**, (3), pp 201–207.
[26] Hampson, M. Drone delivers human kidney: The organ was flown several kilometers by a drone without incurring damage, *IEEE Spectrum*, 2019, **56**, (1), pp 7–9.
[27] Hii, M.S.Y., Courtney, P. and RoyallL, P.G. An evaluation of the delivery of medicines using drones, *Drones*, 2019, 3, (3).
[28] Fossen, T.I. *Guidance and Control of Ocean Vehicles*. *Wiley*, New York, 1994.
[29] Kim, J., Kang, M.S. and Park, S. Accurate modeling and robust hovering control for a quad-rotor Vtol aircraft, *Selected Papers from the 2nd International Symposium on UAVs*, pp 9–26, 2009.
[30] Luukkonen, T. Modelling and control of quadrotor. Independent research project in applied mathematics, *Espoo*, 2011, **22**.
[31] Carrillo, L.R.G., Lopez, A.E.D. and Lozano, R. Quad rotorcraft control: Vision-based hovering and navigation. *Springer Science & Business Media,* 2012.
[32] Martinez, E.H., Anaya, G.F., Ferreira, E.D., Godoy, J.J.F. and Gonzalez, A.L. Trajectory tracking of a quadrotor UAV with optimal translational control, *IFAC-PapersOnLine*, 2015, **48**, (19), pp 226–231.
[33] Shen, X., Fan, J. and Wang, H. Design and simulation of eight-rotor unmanned aerial vehicle based on hybrid control system, *Int J Aerosp Eng*, **2018**, 2018.
[34] Castillo-Zamora, J.J., Gomez, K.A.C, Soto, G.I.P. and Resendiz, J.R. Comparison of PD, PID and sliding-mode position controllers for V-Tail quadcopter stability, *IEEE Access*, 2018, **6**, pp 38086–38096.
[35] Derrouaoui, S.H., Bouzid, Y. and Guiatni, M. Towards a new design with generic modeling and adaptive control of a transformable quadrotor, *Aeronaut J*, 2021, **125**, pp 2169–2199.
[36] Subudhi, C.S. and Ezhilarasi, D. Modeling and trajectory tracking with cascaded PD controller for quadrotor, *Procedia Comput Sci*, 2018, **133**, pp 952–959
[37] Lima, G.V. Modelagem Dinamica e Controle para Navegaçao de um Veiculo Aereo não Tripulado do tipo Quadricoptero, Universidade Federal de Uberlandia, 2015.
[38] Utkin, V.I. *Sliding Modes in Control and Optimization*. *Springer Science & Business Media,* 2013.
[39] Reinoso, M.J., Minchala, L.I., Ortiz, P., Astudillo, D.F. and Verdugo, D. Trajectory tracking of a quadrotor using sliding mode control, *IEEE Latin America Transactions*, 2016, **14**, (5), pp 2157–2166.
[40] Vahdanipour, M. and Khodabandeh, M. Adaptive fractional order sliding mode control for a quadrotor with a varying load, *Aerosp Sci Technol*, 2019, **86**, pp 737–747.
[41] Dorf, R.C. and Bishop, R.H. *Modern Control Systems*, *Pearson*, 2011.
[42] Trentin, J.F.S., Cenale, T.P., da Silva, S. and Ribeiro, J.M.S. Attitude control of inverted pendulums using reaction wheels: Comparison between using one and two actuators, *Proc Inst Mech Eng I J Syst Cont Eng*, 2020, **234**, (3), pp 420–429.

https://doi.org/10.1017/aer.2022.35 Published online by Cambridge University Press

[43] Zhang, C., Zhou, X., Zhao, H., Dai, A. and Zhou, H. Three-dimensional fuzzy control of mini quadrotor UAV trajectory tracking under impact of wind disturbance, 2016 *International Conference on Advanced Mechatronic Systems (ICAMechS)*, pp 372–377, 2016.
[44] Beal, T. Digital simulation of atmospheric turbulence for Dryden and Von Karman Models, *J Guid Cont Dynam*, 1993, **16**, (1), pp 132–138.
[45] Botez, R., Boustani, I., Vayani, N., Bigras, P. and Wong, T. Optimal control laws for gust alleviation, *Can Aeronaut Space J*, 2001, **47**, (1), pp 1–6.
[46] Lv, T., Yang, Y. and Chai, L. Extended state observer based MPC for a quadrotor helicopter subject to wind disturbances, 2019 *Chinese Control Conferenc*, pp 8206–8211, 2019.
[47] Aboudonia, A., Rashad, R. and El-Badawy, A. Time domain disturbance observer based control of a quadrotor unmanned aerial vehicle, 2015 *XXV International Conference on Information, Communication and Automation Technologies (ICAT)*, pp 1–6, 2015.
[48] Scalea, J.R., Retaino, S., Blankenship, G., Bartlett, S.T. and Wereley, N. An initial investigation of Unmanned Aircraft Systems (UAVs) and real-time organ status measurement for transporting human organs, *IEEE J Translat Eng Health Med*, 2018, **6**, pp 1–7.

A.0 Dynamic equations

The general motion of the quadrotor was already described in Equation (1), in which the main matrices were defined as follows [29]:

$$\begin{aligned}
&\mathbf{M}_{\eta c}(\boldsymbol{\eta}_c) = \mathbf{I}_{7\times 7}\\
&\mathbf{C}_{\eta c}(\boldsymbol{\nu}, \boldsymbol{\eta}_c) = \mathbf{J}_c\mathbf{M}_c^{-1}\mathbf{C}_c\mathbf{J}_c^{-1} - \dot{\mathbf{J}}_c\mathbf{J}_c^{-1}\\
&\mathbf{g}_{\eta c}(\boldsymbol{\eta}_c) = \mathbf{J}_c\mathbf{M}_c^{-1}\mathbf{g}_{0c}\\
&\mathbf{K}_{\eta c}(\boldsymbol{\eta}_c) = \mathbf{J}_c\mathbf{M}_c^{-1}\mathbf{K}_c\\
&\boldsymbol{\tau}_{\eta c}(\boldsymbol{\eta}_c) = \mathbf{J}_c\mathbf{M}_c^{-1}\boldsymbol{\tau}
\end{aligned}, \tag{19}$$

where $\dot{\mathbf{J}}_c$ is the derivative of the transformation matrix with respect to time. The main matrices of Equation (19) are shown below:

$$\mathbf{M}_c = diag(m + m_c, m + m_c, m, (I_{xx} + I_{xx}^c), (I_{yy} + I_{yy}^c), (I_{zz} + I_{zz}^c), m_c), \tag{20}$$

where $\mathbf{M}_c$ is the inertial matrix, and the Coriolis matrix $\mathbf{C}_c$ can be expressed as:

$$\mathbf{C}_c = \begin{bmatrix}
0 & -(m+m_c)\omega_z & m\omega_y & 0 & 0 & 0 & m_c\omega_y\\
(m+m_c)\omega_z & 0 & -m\omega_x & 0 & 0 & 0 & -m_c\omega_x\\
-m\omega_y & m\omega_x & 0 & 0 & 0 & 0 & 0\\
0 & 0 & 0 & 0 & 0 & I_1\omega_y & 0\\
0 & 0 & 0 & I_2\omega_z & 0 & 0 & 0\\
0 & 0 & 0 & 0 & I_3\omega_x & 0 & 0\\
-m_c\omega_y & m_c\omega_x & 0 & 0 & 0 & 0 & 0
\end{bmatrix}, \tag{21}$$

where I_1, I_2 and I_3 are the moments of inertia along the x,y,z axes, and were defined as $I_1 = (I_{zz} + I_{zz}^c) - (I_{yy} + I_{yy}^c)$, $I_2 = (I_{xx} + I_{xx}^c) - (I_{zz} + I_{zz}^c)$ and $I_3 = (I_{yy} + I_{yy}^c) - (I_{xx} + I_{xx}^c)$, respectively, where I_{ii} is related to the quadrotor and I_{ii}^c refers to the coupled system moments of inertia ($ii = x, y, z$). In addition, the gravitational vector is defined as $\mathbf{g}_{0c} = \{-mgs\theta\ mgc\theta s\phi\ mgc\theta c\phi\ 0\ 0\ 0\ m_c gc\theta c\phi\}^T$.

A new transformation matrix $\mathbf{J}_c$ is considered by using the relationship $\boldsymbol{\eta}_c = \mathbf{J}_c\boldsymbol{\nu}_c$, where $\mathbf{J}_c$ is defined:

$$\mathbf{J}_c = \begin{bmatrix} \mathbf{J}(\boldsymbol{\eta}) & \mathbf{0}_{6\times 1} \\ \mathbf{j}_n & c\theta c\phi \end{bmatrix}, \tag{22}$$

https://doi.org/10.1017/aer.2022.35 Published online by Cambridge University Press

and $\mathbf{J}(\boldsymbol{\eta})$ is defined as:

$$\mathbf{J}(\boldsymbol{\eta}) = \begin{bmatrix} c\psi c\theta & s\phi s\theta c\psi - c\phi s\psi & c\phi s\theta c\psi + s\psi s\phi & 0 & 0 & 0 \\ s\psi c\theta & s\phi s\theta s\psi + c\phi c\psi & c\phi s\theta s\psi - s\phi c\psi & 0 & 0 & 0 \\ -s\theta & s\phi c\theta & c\phi c\theta & 0 & 0 & 0 \\ 0 & 0 & 0 & 1 & s\phi t\theta & c\phi t\theta \\ 0 & 0 & 0 & 0 & c\phi & -s\phi \\ 0 & 0 & 0 & 0 & s\phi/c\theta & c\phi/c\theta \end{bmatrix}, \tag{23}$$

where $\mathbf{j}_n = \{-s\theta \quad c\theta s\phi \quad 0 \quad 0 \quad 0 \quad 0\}$. For numerical simulations, the second order differential equation Equation (1) can be represented in the state space form as follows:

$$\dot{x}_s(t) = \mathbf{A}_c x_s(t) + \mathbf{B}\mathbf{u}(t) + \mathbf{X}_{gc}, \tag{24}$$

where $x_s = \left\{\dot{\boldsymbol{\eta}}_c \quad \boldsymbol{\eta}_c\right\}^T$ is the state vector, $\mathbf{u}(t) = \left\{\boldsymbol{\tau}_{\eta c} \quad \mathbf{0}_{7\times 1}\right\}^T$ is the input vector, $\mathbf{X}_{\eta c} = \left\{-\mathbf{M}_{\eta c}^{-1}\mathbf{g}_{\eta c} \quad \mathbf{0}_{7\times 1}\right\}^T$ is the state vector of gravity, and the dynamic and input matrices are defined as:

$$\mathbf{A}_c = \begin{bmatrix} -\mathbf{M}_{\eta c}^{-1}\mathbf{C}_{\eta c} & -\mathbf{M}_{\eta c}^{-1}K_{\eta c} \\ \mathbf{I}_{7\times 7} & \mathbf{0}_{7\times 7} \end{bmatrix} \quad \mathbf{B} = \begin{bmatrix} \mathbf{M}_{\eta c}^{-1} \\ \mathbf{0}_{7\times 7} \end{bmatrix}. \tag{25}$$

For the proposed quadrotor modeling, its equations of the motion carrying a payload are used. In order to simplify the mathematical model for the numerical implementation of the controller, the UAV is considered at its hovering condition. At that specific position, $\omega_x \approx \dot{\phi}$, $\omega_y \approx \dot{\theta}$, $\omega_z \approx \dot{\psi}$, yielding the next equations:

$$\begin{aligned} (m+m_c)\ddot{x} &= (c\phi s\theta c\psi + s\psi s\phi)U_1 \\ (m+m_c)\ddot{y} &= (c\phi s\theta s\psi - s\phi c\psi)U_1 \\ m\ddot{z} &= -mg + (c\phi c\theta)U_1 \\ (I_{xx}+\Delta I_{xx})\ddot{\phi} &= ((I_{yy}+\Delta I_{yy}) - (I_{zz}+\Delta I_{zz}))\dot{\theta}\dot{\psi} + U_2\,, \\ (I_{yy}+\Delta I_{yy})\ddot{\theta} &= ((I_{zz}+\Delta I_{zz}) - (I_{xx}+\Delta I_{xx}))\dot{\psi}\dot{\phi} + U_3 \\ (I_{zz}+\Delta I_{zz})\ddot{\psi} &= ((I_{xx}+\Delta I_{xx}) - (I_{yy}+\Delta I_{yy}))\dot{\phi}\dot{\theta} + U_4 \\ m_c\ddot{z}_c &= -m_c g \end{aligned} \tag{26}$$

where m, m_c, I_{xx}, I_{yy}, I_{zz} are the parameters of the controller for the quadrotor with the payload, and ΔI_{xx}, ΔI_{yy} and ΔI_{zz} are parameters related to the uncertainties dues to the payload dynamics added to the quadrotor dynamics. The equations of motion can also be rewritten as $\ddot{k} = f_k + g_k U_j + \Delta f_k$, (such that $k = x, y, z, \phi, \theta, \psi, z_c$ and $j = 1, 2, 3, 4$). For instance, the second-order derivative of roll $\ddot{\phi}$ is expressed with next formulation $\ddot{\phi} = [(\dot{\theta}\dot{\psi}(I_{yy} - I_{zz}))/I_{xx}] + [1/I_{xx}]U_2 + [-(\dot{\theta}\dot{\psi}(I_{yy} - I_{zz}) + U_2)\Delta I_{xx}/[I_{xx}(I_{xx} + \Delta I_{xx})] + \dot{\theta}\dot{\psi}(\Delta I_{yy} - \Delta I_{zz})(I_{xx} + \Delta I_{xx})]$.

B.0 Dryden gust modeling

Section 2.3 shows the Dryden gust turbulence equations in z direction shows the Dryden gust turbulence equations in the z direction. The Power Spectral Densities (PSD) of the turbulence velocities in the x and y directions are expressed as:

$$\Phi_x(\Omega) = \sigma_x^2 \frac{2L_x}{\pi} \frac{1}{1 + (L_x\Omega)^2}, \tag{27}$$

$$\Phi_y(\Omega) = \sigma_y^2 \frac{L_y}{\pi} \frac{1 + 3(L_y\Omega)^2}{(1 + (L_y\Omega)^2)^2}, \tag{28}$$

https://doi.org/10.1017/aer.2022.35 Published online by Cambridge University Press

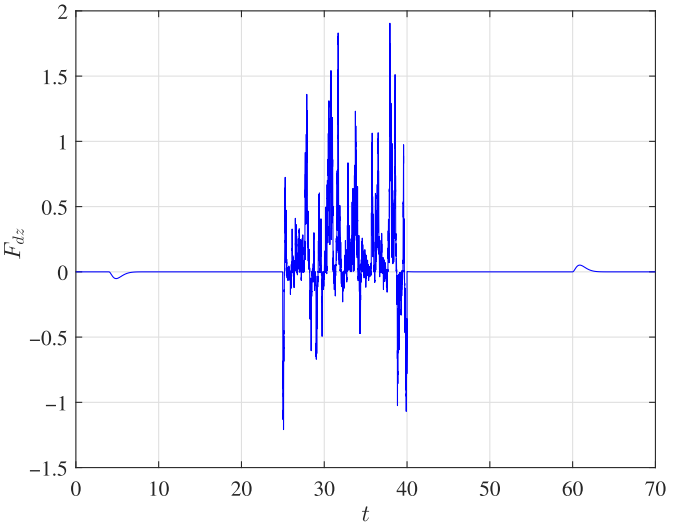

Figure 15. *Wind disturbance force generated by the Dryden gust oriented in the z direction.*

where the turbulence scale length and intensity in the x and y directions can be defined as shown below:

$$L_x = \frac{h}{(0.177 + 0.000823h)^{1.2}} \quad \sigma_x = \frac{\sigma_z}{(0.177 + 0.000823h)^{0.4}}, \tag{29}$$

where $L_y = L_x$ and $\sigma_y = \sigma_x$. The transfer functions of shaping filters on their directions are expressed as:

$$\begin{aligned} G_x(s) &= \frac{v_{x_d(s)}}{\eta_x(s)} = \sigma_x \sqrt{\frac{2L_x}{\pi V}} \frac{1}{1 + \frac{L_x}{V}s}, \\ G_y(s) &= \frac{v_{y_d(s)}}{\eta_y(s)} = \sigma_y \sqrt{\frac{L_y}{\pi V}} \frac{1 + \frac{\sqrt{3}L_y}{V}s}{\left(1 + \frac{L_y}{V}s\right)^2}. \end{aligned} \tag{30}$$

The wind velocities in the inertial reference frame can be represented using two equations $v_{wx} = \bar{v}_{wx} + v_{x_d}$ and $v_{wy} = \bar{v}_{wy} + v_{y_d}$. Moreover, the proposed wind modeling is used in numerical simulations to obtain the external disturbances impact on the quadrotor motion. Thus, the wind force generated by use of Dryden equations can be shown on Fig. 15 during an interval of time between 25 and 40s.

C.0 Adapted controller

The "total thrust" is the force required to lift the quadrotor and its payload. The quadrotor is functioning only in its vertical direction z (the full equation of motion is used for the control law design), while for the proposed model, it is necessary to combine the vertical equations of motion for both systems, including $\ddot{z}$ and $\ddot{z}_c$ accelerations, as follows:

$$m\ddot{z} + mg + m_c\ddot{z}_c + m_c g = (c\phi c\theta)U_1, \tag{31}$$

where $\ddot{z}_c = \ddot{z} + \delta$, such that the acceleration difference is $\delta = \ddot{z}_c - \ddot{z}$. In order to design the control law in the z direction, it is assumed that $\delta = 0$ (since the control is needed for guiding the quadrotor with its payload at the reference altitude z). Therefore, the new controller equation for the vertical direction is defined as $(m + m_c)(\ddot{z} + g) = (c\phi c\theta)U_1$, in which for convenience $m + m_c$ is replaced by $\tilde{m}$. The total

https://doi.org/10.1017/aer.2022.35 Published online by Cambridge University Press

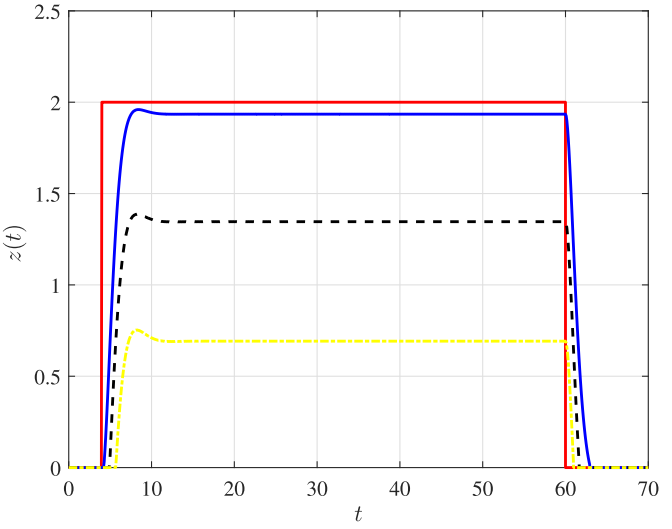

Figure 16. *Trajectory influenced by the value of the attached mass m_c, where the desired trajectory (solid red line −), $m_c = 0.022$ (solid blue line −), $m_c = 0.22$ (dashed black line −−), and $m_c = 0.44$ (dash-dotted yellow line −.).*

thrust of motors using the Sliding Mode Control (SMC) is represented by:

$$U_{1c} = \frac{\tilde{m}}{c\theta c\phi}(\epsilon_z sat(s_z) + \eta_z s_z + \lambda_z(\dot{e}_z) + \ddot{z}_{des} + g). \tag{32}$$

Overall, the conventional control does not take into account the effect of the attached mass, because of the fact that the only mass that needs to be lifted is that of the quadrotor itself. Figure 16 shows the impact of the extra mass attached to the quadrotor on its tracking trajectory using the conventional input control U_{1c}. The load masses range from 1% to 20% of the quadrotor mass.

As seen on Fig. 16, the value of the load affects directly the altitude reached by the quadrotor, when $\tilde{m} = m$. Increasing the gain value of the controller or the propeller velocity are two of the possible solutions adopted to compensate the loss in altitude. Thereby, besides spending more energy to fit the proposed trajectory, the vibration level might be increased (since the propellers velocities are increased), decreasing the quadrotor performance. A compensation in the controller is proposed to maintain the quadrotor stability and the desired altitude, defined as $\tilde{m} = m + m_c$. Therefore, by using this procedure, the quadrotor keeps the desired altitude regardless of the extra mass added to the system.

Cite this article: Geronel R. S., Botez R. M. and Bueno D. D. (2023). Dynamic responses due to the Dryden gust of an autonomous quadrotor UAV carrying a payload. *The Aeronautical Journal*, **127**, 116–138. https://doi.org/10.1017/aer.2022.35